Chinese Journal of
POLYMER SCIENCE

RESEARCH ARTICLE

• 2026 Rising Scholars •

https://doi.org/10.1007/s10118-026-3804-5
Chinese J. Polym. Sci.

A Multidimensional and Multinuclear Nuclear Magnetic Resonance Spectroscopy Strategy for Fine Structural Elucidation of Perhydropolysilazane

Li-Fei Yuan[a,b], Qian Li[d], Hui-Yuan Yang[a,b], Ji-Lei Chen[a,b], Ding-Yu Hou[c], Peng-Fei Li[a*], Cai-Hong Xu[a], and Zong-Bo Zhang[a*]

[a] *Key Laboratory of Science and Technology on High-tech Polymer Materials, Institute of Chemistry, Chinese Academy of Sciences, Beijing 100190, China*
[b] *University of Chinese Academy of Sciences, Beijing 100149, China*
[c] *Beijing National Laboratory for Molecular Sciences, State Key Laboratory of Polymer Physics and Chemistry, Institute of Chemistry, Chinese Academy of Sciences, Beijing 100190, China*
[d] *Center for Physicochemical Analysis and Measurements, Institute of Chemistry, Chinese Academy of Sciences, Beijing 100190, China*

Electronic Supplementary Information

Abstract Perhydropolysilazane (PHPS) is a silicon-nitrogen backbone polymer widely utilized as a ceramic precursor; however, a deep understanding of its molecular structure has been hindered by the complex and highly branched architecture. This work presents a systematic and quantitative investigation into the molecular structure of PHPS by integrating advanced characterization techniques, including multidimensional nuclear magnetic resonance spectroscopy (^{1}H-/ ^{29}Si-/ ^{15}N-NMR), gel permeation chromatography with multi-angle light scattering and differential viscometry (GPC-MALS-Vis), and molecular simulations. Through multidimensional NMR analysis, five fundamental structural units (—SiH, —SiH_2, —SiH_3, —NH, and —N) were identified, with no detectable —NH_2 groups. A dual-nucleus quantification strategy based on ^{1}H- and ^{29}Si-NMR enabled the precise determination of the molar ratios of these structural units. Building upon these results, two structural parameters—branching degree (D_b) and number of cyclization (N_c)—were introduced to quantitatively characterize the network topology of PHPS. Subsequently, three-dimensional molecular models were constructed *via* density functional theory (DFT) simulations to reveal the micro-conformations of the polymer. This study establishes a robust characterization framework that reveals the fine structure and network topology of PHPS, thereby providing a significant theoretical foundation and technical support for structural tailoring and performance optimization to meet the demanding requirements of integrated circuits, functional coatings, and advanced functional materials.

Keywords Perhydropolysilazane; Structural characterization; Nuclear magnetic resonance (NMR); Branching degree; Number of cyclization

Citation: Yuan, L. F.; Li, Q.; Yang, H. Y.; Chen, J. L.; Hou, D. Y.; Li, P. F.; Xu, C. H.; Zhang, Z. B. A multidimensional and multinuclear nuclear magnetic resonance spectroscopy strategy for fine structural elucidation of perhydropolysilazane. *Chinese J. Polym. Sci.* https://doi.org/10.1007/s10118-026-3804-5

INTRODUCTION

Perhydropolysilazane (PHPS)[1,2] is an inorganic polymer comprising a Si—N backbone with hydrogen substituents, representing a major branch within the polysilazane family. Research on PHPS traces back to 1921,[3] when Stock and Somieski synthesized a low-molecular-weight polysilazane (M_n≈350) *via* ammonolysis of dichlorosilane in benzene. Owing to its limited molar mass and high chemical reactivity, this early oligomer exhibited significant instability at room temperature, rapidly transforming into a transparent, glass-like solid through hydrolysis and condensation within 24 h. Subsequently, Seyferth *et al.*[4] optimized the synthesis by employing polar solvents, such as diethyl ether or dichloromethane, yielding soluble and non-volatile liquid polysilazanes. These improved precursors underwent progressive crosslinking under ambient air to thicken and eventually solidify into dense glassy materials. In recent years, commercially available PHPS has emerged in market due to the maturity of the synthetic method.[5,6]

Currently, PHPS has been established as a key solution-processable precursor for the fabrication of both silicon nitride (Si_3N_4) ceramics[7] and dense inorganic silica films[8], particularly for achieving uniform coatings on large-area or topographically complex substrates.[9–12] The transformation of PHPS into a dense SiO_2 network is achievable through various conversion pathways, including thermal treatment,[13,14] catalytic routes,[15] and ultraviolet irradiation.[9,12,16–18] Furthermore, PHPS exhibits excellent interfacial affinity toward

* Corresponding authors, E-mail: lpf2017@iccas.ac.cn (P.F.L.)
E-mail: zongbo@iccas.ac.cn (Z.B.Z.)
Received May 27, 2026; Accepted July 5, 2026; Published online September 16, 2026

substrates such as glass, ceramics, steel, and polymers, allowing its molecular architecture to be tailored for diverse functional requirements.[19–22] These versatile properties have facilitated the extensive implementation of PHPS-derived SiO_2 in microelectronics,[23,24] metal protection,[22,25,26] optical coatings,[27,28] and gas barrier applications.[29,30]

Serving as a pivotal bridge linking the synthetic pathways and functional performance, the molecular structure of a polymer represents both the culmination of specific reaction conditions and the primary factor governing its final application properties[31]. Although the practical applications of PHPS have been widely explored, their detailed fine structure remains insufficiently defined. This ambiguity stems from its intricate three-dimensional (3D) topological network, characterized by profound complexity and polydispersity, coupled with its inherent sensitivity to environmental conditions. Consequently, although various conventional characterization methods have been explored, the current understanding of PHPS structures remains largely qualitative. This limitation significantly constrains the further enhancement of its performance and precise regulation of synthetic parameters.

For instance, Bender *et al.*[32] performed molecular analyses using nuclear magnetic resonance (NMR) and light scattering (LS), revealing a predominance of polycyclic motifs with irregular topologies and complex nonlinearity. Although these findings established a foundation for polysilazane research, they remained largely descriptive. Subsequently, Chen *et al.*[33] utilized Fourier-transform infrared spectroscopy (FTIR), gel permeation chromatography (GPC), and pyrolysis-gas chromatography/mass spectrometry (PY-GC/MS) to monitor the structural evolution during thermal polymerization, and proposed a mechanism based on Si—H/N—H dehydrocoupling followed by cyclization. However, their findings provided limited insight into the fine structure of PHPS and remained predominantly qualitative. Similarly, Barysheva *et al.*[34] systematically investigated the effect of ammonia flow rates and observed that ammonia supply significantly influences linkage patterns and branching. Nevertheless, these inferences were derived from qualitative spectral signatures and molar mass distributions rather than from precise, quantitative fine structure resolution.

The limited understanding of the fine structure of PHPS has emerged as a critical scientific challenge and technical bottleneck for its advancement in fields such as microelectronics. To address these issues, the present study establishes a refined analytical methodology for the molecular structure of PHPS. By integrating multinuclear and multidimensional NMR spectroscopy, including ^{1}H-NMR, ^{29}Si-NMR, ^{29}Si-DEPT (Distortionless Enhancement by Polarization Transfe), ^{15}N-DEPT, 2D ^{1}H-^{29}Si HSQC (Heteronuclear Single Quantum Coherence), and 2D ^{1}H-^{15}N HSQC) with GPC-MALS-Vis and DFT molecular simulations, we identified the fundamental structural units of PHPS and constructed a molecular analysis framework based on the synergistic constraints of local chemical environments and global conformations. Building on this, a quantitative strategy was developed to transform the molar ratios and connectivity features of these structural units into calculable statistical parameters. Specifically, the degree of branching (D_b) and number of cyclization (N_c) were defined to facilitate a consistent cross-sample evaluation system. This unified approach not only enables the reliable characterization of PHPS from various sources, but also provides a solid theoretical and experimental foundation for further exploration of its structure-property relationships.

EXPERIMENTAL

Reagents and Materials

Analytical grade dichlorosilane (SiH_2Cl_2, ≥99%, Tangshan Sanfu), anhydrous pyridine (≥99%, Aladdin), dibutyl ether (≥99%, SuperDry, J&KSeal), and anhydrous ammonia gas (NH_3, 99.999%, Credit) were of analytical grade. All the procedures were conducted under an inert nitrogen atmosphere to prevent moisture and oxygen contamination of the products.

Synthesis of PHPS

PHPS was synthesized *via* a typical ammonolysis route.[35] A standard procedure is described as follows. In a pressure-resistant glass reactor, 500 g of pyridine was added as the solvent and cooled to the desired temperature. Subsequently, 10 L of dichlorosilane was added at a constant rate of 100 mL/min, followed by the introduction of 50 L of anhydrous ammonia under isothermal conditions within 3 h. After the reaction, dry nitrogen was passed through the system for 1.5 h to remove the residual ammonia. The mixture was filtered through a 0.1 μm PTFE pressure filter to obtain the crude product. Pyridine was removed by triple treatment with anhydrous *n*-butyl ether (DBE) and rotary evaporation. The resulting PHPS solution was diluted to 20 wt% by varying the synthesis procedure to obtain nine different PHPS samples, named P-1–P-5 and S-1–S-4, respectively.

Characterization

GPC-MALS-Vis

The molecular weight distribution and branching characteristics of the PHPS were determined using a GPC system equipped with a Wyatt DAWN HELEOS-II multi-angle laser light scattering (MALS) detector (Wyatt Technology, USA) and a ViscoStar III differential viscometer. Separation was carried out using a set of three Styragel HR columns (HR1, HR3, and HR5; 7.8 mm × 300 mm, 5 μm particle size, Waters) maintained at 35 ℃, with tetrahydrofuran (THF) as the mobile phase at a constant flow rate of 1.0 mL·min^{-1}. Prior to injection, PHPS samples were dissolved in THF (2–3 mg·mL^{-1}), filtered through a 0.22 μm PTFE syringe filter, and allowed to equilibrate. The d*n*/d*c* value of PHPS in THF was experimentally determined to be 0.1253 mL·g^{-1}, and used in molecular weight calculations. Data were processed using the ASTRA software (v7.3, Wyatt Technology). The Mark-Houwink-Sakurada equation was applied to determine the intrinsic viscosities and infer the branching behavior. The slope deviation in the double logarithmic plot of intrinsic viscosity versus molecular weight was used as a qualitative indicator of branching density.

NMR spectroscopy

All NMR experiments were carried out on a Bruker Avance NEO 700 MHz superconducting spectrometer equipped with a 5 mm broadband double-resonance cryoprobe and z-gradient system, operating at 298 K. Anhydrous *n*-butyl ether was used as the solvent (pre-dried over molecular sieves).

The ^{1}H-NMR spectrum was obtained using the raw PHPS-

pyridine solution diluted with $CDCl_3$ (final concentration of 1 wt%). The acquisition parameters included 8–16 scans for ^1H.

Unless otherwise specified, all the PHPS samples were dissolved in *n*-butyl ether (DBE). A concentration of 35 wt% was used for all quantitative measurements, except for several reference samples prepared at 15 wt%. All solutions were filtered through 0.22 um PTFE filters prior to measurement, and the following NMR experiments were performed:

1D ^{29}Si- and 1D ^1H-NMR spectroscopy were conducted to quantify the —SiH, —SiH_2, and —SiH_3 units. Acquisition parameters included relaxation delay (D1) of 30 s for ^{29}Si, 64–256 scans for ^{29}Si (depending on signal-to-noise), and 8–16 scans for ^1H.

^1H-^{29}Si HSQC NMR was optimized for ^1H-^{29}Si single bond *J*-couplings to assign Si—H correlations.

^{15}N-DEPT NMR experiments (pulse angles of 45°, 90°, and 135°) were used to distinguish between the primary —NH_2 and secondary —NH groups. Typical acquisitions used NS = 128–256 and relaxation delay = 2 s.

^1H-^{15}N HSQC NMR was used to probe ^1H-^{15}N couplings associated with Si—N—H linkages, providing insights into nitrogen coordination and chain branching. The parameters included 1024 × 128 complex points with zero filling in F1.

^1H-^{15}N HMBC NMR was employed to probe long-range (^2J and ^3J) ^1H-^{15}N heteronuclear couplings, enabling the identification of through-bond connectivity between nitrogen and remote proton environments and providing complementary information on nitrogen coordination and chain connectivity. Spectra were recorded with 1024 × 128 complex points, with zero-filling applied in the F1 dimension to improve the digital resolution.

^{29}Si-DEPT-135° NMR was conducted to differentiate the primary, secondary, and tertiary silicon environments, aiding in the analysis of branching topologies. ^{29}Si spectra were recorded with NS=128, D1=2 s, and inverse-gated decoupling to ensure a quantitative signal acquisition.

For all quantitative NMR measurements, long relaxation delays (≥30 s) were employed to ensure full spin relaxation, particularly for ^{29}Si and ^{15}N nuclei. Signal integration was performed using the MestReNova software. The molar fractions of —SiH, —SiH_2, and —SiH_3 units were calculated based on integrated peak areas and normalized using dual-nuclear integral ratios.

Molecular Simulation

We constructed multiple candidate molecular structures for each configuration, based on the experimentally determined ratios of the structural units. Initial geometry optimization was performed using the RDKit implementation of the Universal Force Field (UFF)[36] *via* AllChem. UFF Optimize Molecule (mol) in Python. The resulting structures were then further optimized in Gaussian 16[37] using the semiempirical PM6[38] method and density functional theory (DFT) at the B3LYP/6-31G(d) level. Finally, the structure with the lowest energy among the optimized candidates was selected.

Validation of Characterization Methodology

To verify the accuracy of the characterization strategy for the PHPS fine structure, several model compounds and reference PHPS samples (S-1–S-4) were selected for experimental validation. The corresponding data are provided in Figs. S1–S6 (in the electronic supplementary information, ESI) within Parts 1–3. The detailed discussions regarding the feasibility and accuracy of these methods are provided in the **RESULTS AND DISCUSSION** section.

RESULTS AND DISCUSSION

Preliminary Theoretical Analysis of Characteristic Structural Units in PHPS

PHPS is composed of Si, N, and H, with a backbone consisting of Si—N bonds and hydrogen pendants attached to the Si and N atoms. As illustrated in Fig. 1(a), PHPS was synthesized *via* the low-temperature ammonolysis of dichlorosilane (DCS) in pyri-

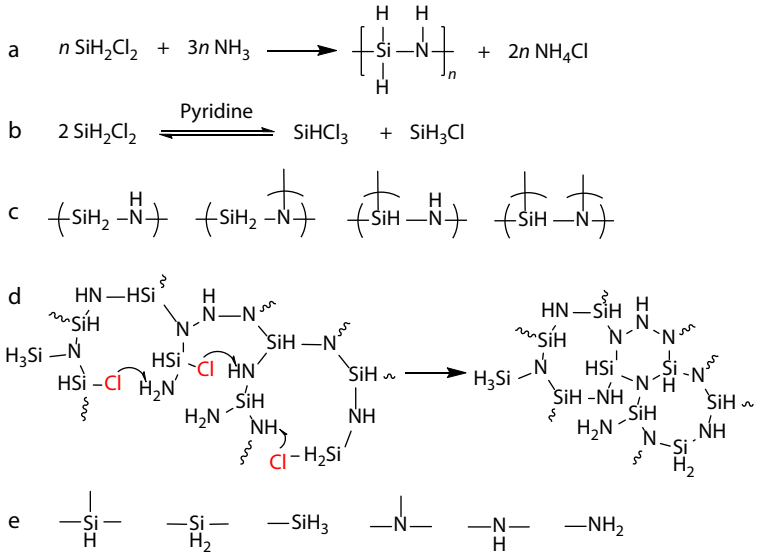

Fig. 1 (a) Schematic illustration of the synthetic reaction of PHPS; (b) The disproportionation reaction of dichlorosilane; (c) The possible Si—N diatomic linkage units in the PHPS molecular backbone; (d) The possible cyclization mechanisms during the chain growth process of PHPS; (e) Six potential structural units in PHPS.

https://doi.org/10.1007/s10118-026-3804-5

dine.[39,40] In this reaction, pyridine serves as both a solvent and Lewis base, catalyzing the disproportionation of DCS into two distinct chlorosilane monomers that subsequently participate in the ammonolysis process (Fig. 1b).[41] Owing to the presence of excess ammonia, the Si—Cl bonds are completely consumed, resulting in various Si—N dual-linkage combinations (Fig. 1c). Consequently, the conventional —SiH_2—NH— repeating unit model is insufficient to accurately characterize the complex chain conformations of PHPS.

During chain propagation, intramolecular condensation between the residual Si—Cl bonds and adjacent N—H groups leads to the formation of localized cyclic structures (Fig. 1d).[40]

According to structural chemistry and ring strain analysis,[42] six- and eight-membered rings exhibit high thermodynamic stability in silicon-nitrogen systems.[43] This suggests that the actual configuration of PHPS favors the formation of a three-dimensional network architecture primarily composed of these silazane ring units. However, the understanding of the PHPS architecture has long been restricted to theoretical inferences, with a distinct lack of refined experimental characterization. To address this bottleneck, we propose a "characteristic atom-centered structural unit" approach, where the PHPS framework can be deconstructed into six potential structural units (Fig. 1e): three N-centered units (—N, —NH, —NH_2) and three Si-centered units (—SiH, —SiH_2, —SiH_3). Through quantitative investigation of the distribution of these units, it is possible to further elucidate the ring proportion and fine molecular structure within PHPS.

Identification and Assignment of Si-centered Structural Units

As illustrated in Fig. 2, three Si-centered structural units were identified using 2D ^{1}H-^{29}Si HSQC NMR spectroscopy. Influenced by the conformational distribution of the polymer, the Si—H bond signals exhibit characteristic broad peaks.[44] Specifically, signals situated in the low-field region, centered at (F2, F1) approx. (4.75, –32.50) ppm, with peak widths primarily distributed across F2 approx. 4.50–5.10 ppm and F1 approx. –40.00 to –23.00 ppm—are assigned to the overlap of the —SiH and —SiH_2 units.[45–47] Due to a more pronounced chemical shielding effect, the signal corresponding to the —SiH_3 unit is located in the high-field region, centered at (F2, F1) approximately. (4.25, –50.00) ppm, with peak widths ranging from F2 approx. 4.10 ppm to 4.50 ppm and F1 approx. –55 to –40 ppm. The full-scale version of the spectrum in Fig. 2 is provided in Fig. S7 (in ESI).

Identification and Assignment of N-centered Structural Units

PHPS is synthesized in pyridine and commonly undergoes solvent exchange into DBE for film deposition and subsequent silica conversion. Because of the resonance overlap between the C—H bonds of DBE and the N—H environment of PHPS in ^{1}H-NMR, the spectrum in Fig. 3 was recorded using the original PHPS-pyridine solution diluted with $CDCl_3$. The full-scale version of the spectrum in Fig. 3 is provided in Fig. S8 (in ESI). This avoids the interference associated with the DBE and allows for unambiguous identification of the N—H units. As depicted in the ^{1}H-NMR spectrum (Fig. 3), a broad resonance centered at approximately 1.60 ppm is assigned to the N—H bond, encompassing

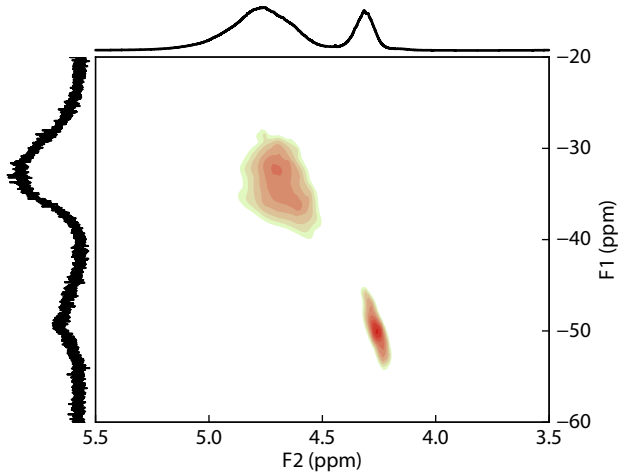

Fig. 2 ^{1}H-^{29}Si HSQC spectrum of PHPS (P-1).

—NH and potentially —NH_2 units. However, the presence of tertiary nitrogen centers (—N units) cannot be definitively confirmed *via* 1D ^{1}H-NMR alone. To resolve this ambiguity, a comparative analysis of ^{1}H-^{15}N HSQC and HMBC experiments was performed, using sample P-5 as a representative case. HSQC, which relies on one-bond heteronuclear correlations ($^1J_{N–H}$), exclusively identifies nitrogen atoms directly bonded to hydrogen.[48] As shown in the red box in Fig. 4(a), cross-peaks corresponding to the —NH and —NH_2 units appear within the ^{15}N chemical shift (F1) range of 20–48 ppm. In contrast, HMBC captures long-range correlations ($^2J/^3J_{N–H}$), enabling the detection of nitrogen centers coupled to more distant protons, such as those in the Si—H groups.[49] While all N-centered units (—N, —NH, and —NH_2) are theoretically observable in HMBC, the —N units can be unambiguously identified by isolating the signals that appear in the HMBC spectrum but fall outside the F1 range established by HSQC (Fig. 4b, red box).

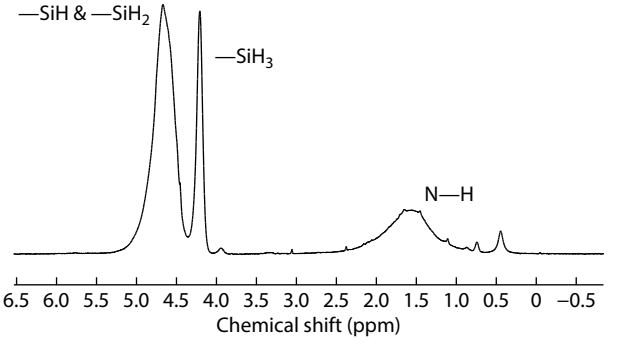

Fig. 3 ^{1}H-NMR spectrum of PHPS pyridine solution diluted with $CDCl_3$.

Given the high reactivity of the —NH_2 units during PHPS synthesis, their persistence in the final product warrants rigorous verification. To this end, ^{15}N-DEPT NMR was employed to differentiate the primary (—NH_2) and secondary (—NH) amine groups based on their distinct phase responses at varying pulse angles (45°, 90°, and 135°). As summarized in Fig. 5(f), under a 135° pulse, because of their distinct coupling evolution, the —NH and —NH_2 groups exhibit different phase responses under varying pulse angles.[50] As shown in

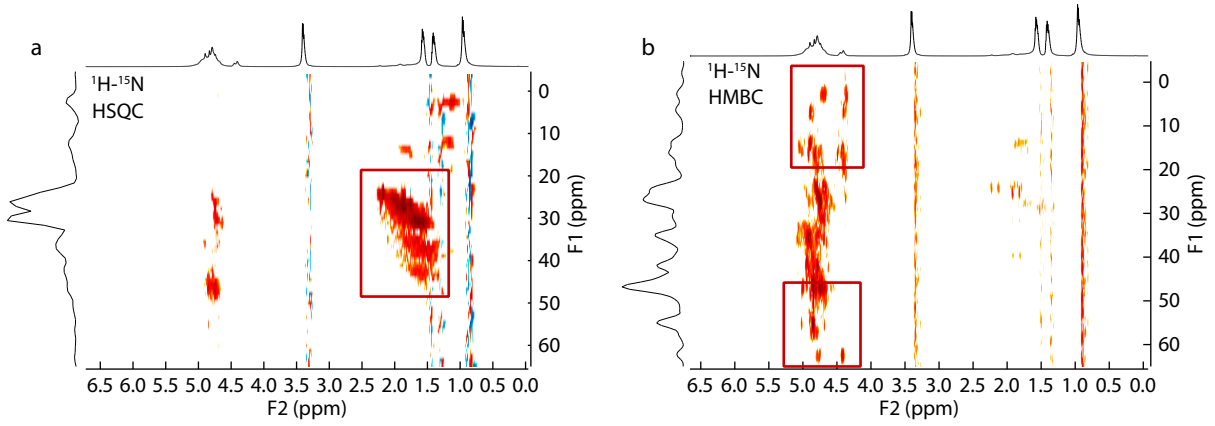

Fig. 4 (a) ^{1}H-^{15}N HSQC NMR spectrum of P-5; (b) ^{1}H-^{15}N HMBC NMR spectrum of P-5.

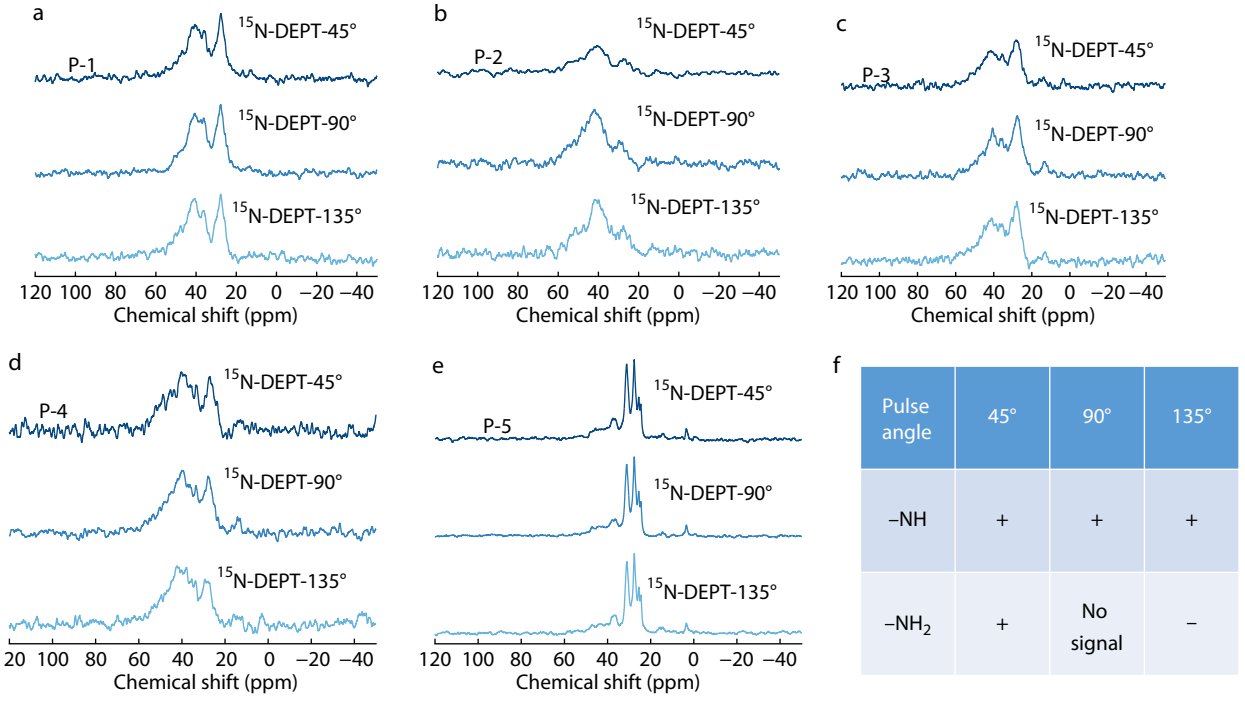

Fig. 5 ^{15}N DEPT NMR spectra of PHPS samples: (a–e) ^{15}N DEPT spectra of samples P-1 to P-5 at various pulse angles (45°, 90°, and 135°); (f) Schematic illustration of the phase responses for —NH and —NH$_2$ groups at different pulse angles (where "+", "–", and "No signal" denote positive, negative, and absent signals, respectively).

Figs. 5(a)–5(e), the experimental results across all five PHPS samples revealed highly consistent spectra with no negative signals or characteristic resonances corresponding to the —NH$_2$ units. This lack of primary amine signals confirms that the N-centered units consist exclusively of —NH and —N. Consequently, it is established that PHPS is composed of five fundamental structural units: three silicon centers (—SiH, —SiH$_2$, and —SiH$_3$) and two nitrogen centers (—N and —NH). This definitive identification of the constituent units provides the essential groundwork for subsequent fine-structure quantification.

Preliminary Investigation on the Branching Degree of PHPS Fine Structure

Because —SiH and —N units function as T-type branching nodes within the backbone, their relative proportions dictate the branching degree of the PHPS. However, quantitative analysis of these branching nodes presents significant challenges. On the one hand, the substantial overlap between —SiH and —SiH$_2$ signals in ^{1}H-^{29}Si HSQC spectra, exacerbated by conformational complexity and peak broadening, precludes accurate quantification *via* conventional peak fitting. However, —N units cannot be detected by ^{1}H-NMR because of the lack of directly attached protons. Moreover, their characterization *via* ^{15}N-NMR is severely limited by the low natural abundance of ^{15}N and a substantial chemical shift overlap with the —NH units.[51,52] Consequently, direct integration of ^{15}N-NMR signals for branching analysis remains impractical.

To circumvent these hurdles, a cross-verification strategy integrating ^{29}Si-DEPT-135, ^{1}H-^{15}N HSQC, and GPC-MALS-Vis was implemented to qualitatively evaluate the branching de-

gree of the PHPS.

As illustrated in the ^{29}Si-DEPT-135° spectra (Fig. 6), the —SiH and —SiH_2 units exhibited positive and negative phase signals, respectively.[53] Although their chemical shifts overlap within the range from –24 ppm to –44 ppm, the "net negative peak" resulting from phase cancellation reflects the relative content of —SiH_2 with respect to —SiH. The —SiH_3 units (–44 to –56 ppm) exhibit an independent peak. By normalizing the —SiH_3 peak area across different samples, the branching degree of PHPS can be qualitatively assessed: smaller net negative —SiH/—SiH_2 peak indicates a higher degree of compensation from the positive —SiH signal, corresponding to a higher —SiH content relative to —SiH_3 and a more highly Si-centered branching degree. Comparison of the normalized spectra revealed distinct variations among the five PHPS samples. Based on the decreasing order of the net negative —SiH/—SiH_2 peak, the Si-centered branching degree was ranked as follows: P-5 < P-1 ≈ P-3 < P-4 < P-2.

To gain deeper qualitative insights into the branching characteristics of Si-centered units, ^{1}H-^{15}N HSQC was employed. As shown in Fig. 7, the relative intensities of the two N—H correlation cross peaks reflect the local chemical environment of the Si atoms adjacent to the —NH linkages. As established in Part 1 of ESI and supported by the experimental data in Fig. S1 and Table S1 (in ESI), the resonances within the 20.0–32.5 ppm range in the F1 dimension are primarily assigned to —NH units neighboring non-branched silicon centers, such as —SiH_2 and —SiH_3. This assignment stems from the enhanced electronic shielding effect, which is a characteristic of lower chemical shifts. Conversely, the resonance within 32.5–57.5 ppm (F1) corresponds to —NH units neighboring branched Si-centers units (defined as "NH units with branched Si neighbors") (Fig. 7f).

As illustrated in Figs. 7(a)–7(e), sample P-2 exhibits the highest relative intensity of the branched Si-neighboring NH peak compared to its non-branched counterpart, indicating the highest degree of branching at the Si-centered units. In contrast, sample P-5 shows the lowest relative intensity, reflecting the minimum degree of branching at the Si-centered units. The relative intensities for the remaining samples follow the increasing order: P-5 < P-1 ≈ P-3 < P-4 < P-2. These findings are in agreement with the conclusions derived from the ^{29}Si-DEPT-135° spectra. The convergence of the results provides robust cross-validation, achieving a multidimensional qualitative assessment of the branching fine structure in the PHPS.

Following the qualitative assessment of Si-centered branching, the challenge remains to quantify the N-centered branching units (—N) directly *via* NMR. Consequently, GPC-MALS-Vis was employed to indirectly evaluate the branching derived from both —SiH and —N by analyzing the differences in the chain conformation. This approach is predicated on the impact of the branching architecture on the compactness of polymer chains, as described by the Mark-Houwink-Sakurada (MHS) equation (Eq. 1).[54–56]

$$[\eta] = KM^{a} \quad (1)$$

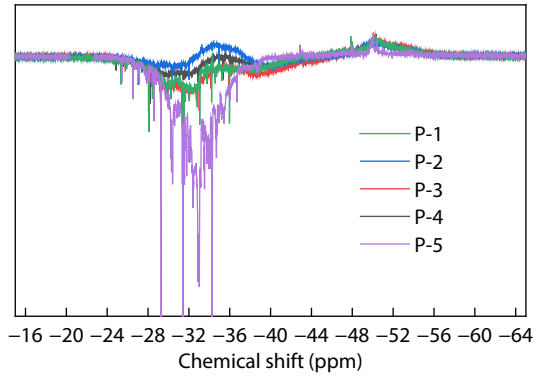

Fig. 6 ^{29}Si-DEPT-135° NMR spectra of P-1–P-5.

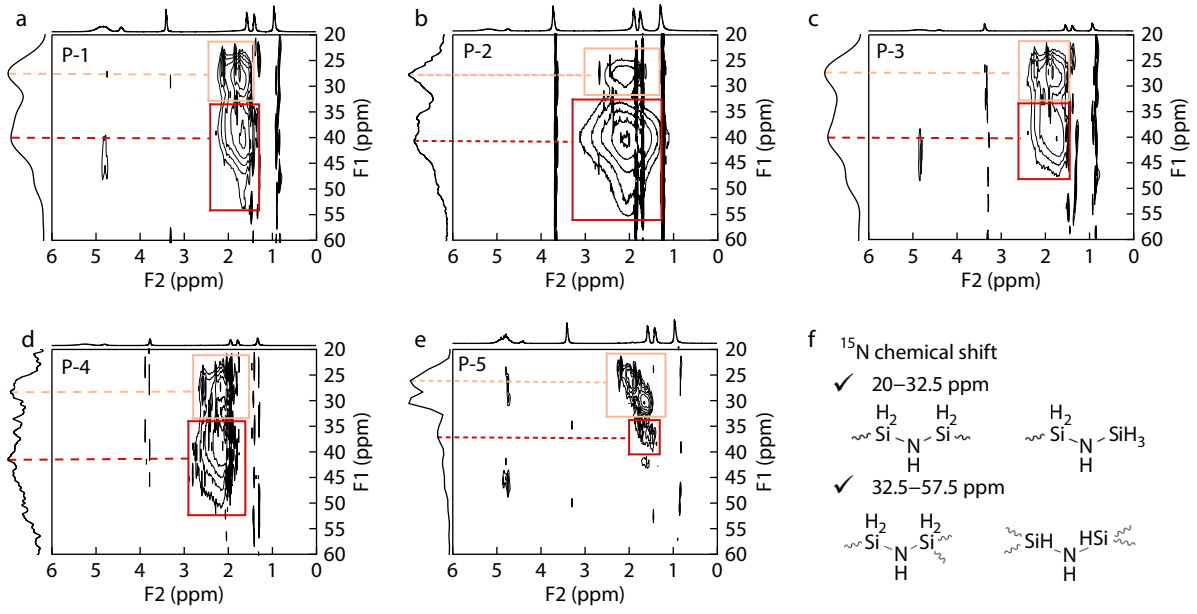

Fig. 7 (a–e) Two-dimensional ^{1}H-^{15}N HSQC NMR spectra of samples P-1 to P-5; (f) Schematic assignment of —NH cross-peaks with neighboring Si environments in the ^{15}N chemical-shift regions of 20.0–32.5 ppm and 32.5–57.5 ppm.

https://doi.org/10.1007/s10118-026-3804-5

The parameter K is a proportionality constant characteristic of a specific polymer-solvent system at a defined temperature. The α, which relates the intrinsic viscosity (η) to the absolute molecular weight M, serves as a sensitive indicator of polymer chain conformation. Generally, a lower α value reflects a more compact hydrodynamic volume, suggesting a higher degree of branching, whereas a higher α value indicates a more extended or linear conformation. Thus, as shown in Figs. 8(a)–8(f), comparing the α values of the different PHPS samples allows for a qualitative ranking of their branching degree (P-2 > P-4 > P-3 > P-1 > P-5).

At this stage, a preliminary investigation of the branching degree of the PHPS fine structure was conducted.

Quantitative Characterization Strategy for the Fine Structure of PHPS

As shown in ^{1}H-^{29}Si HSQC, the resonances for the —SiH and —SiH_2 units exhibit significant overlap, whereas the —SiH_3 signal remains well resolved and distinct. By acquiring quantitative ^{1}H- and ^{29}Si-NMR spectra for the same sample, the relative integral areas of these resonances could be extracted to establish a quantitative structural model. Specifically, the integral ratio in the ^{1}H-NMR spectrum reflects the molar ratio of protons in the combined (—SiH/—SiH_2) environment relative to those in the —SiH_3 unit. Correspondingly, the integral ratio in the ^{29}Si-NMR spectra reveals the molar ratio of the respective Si nuclei. By coupling these dual-nuclear integral ratios, the individual molar fractions of the three Si-centered moieties (—SiH, —SiH_2, and —SiH_3) can be mathematically resolved.

The derivation of this quantitative model is as follows: consider a PHPS sample containing A, B, C, D and E moles of —SiH, —SiH_2, —SiH_3, —NH and —N, respectively. Let "h" represent the relative ^{1}H integral area ratio of the (—SiH/—SiH_2) overlap to the —SiH_3 resonance, and "s" represent the corresponding ratio in the ^{29}Si-NMR spectrum. Based on the fundamental relationship between peak area and atom count, a system of linear equations is established (Eqs. 2 and 3).

$$\frac{A+2B}{3C} = h \tag{2}$$

$$\frac{A+B}{C} = s \tag{3}$$

To facilitate cross-sample comparison, the proportions of these structural units are normalized to —SiH_3 (where C=1). Solving this system yields Eqs. (4) and (5), which represent the molar ratios of —SiH and —SiH_2 relative to —SiH_3, respectively.

$$\frac{A}{C} = 2s - 3h \tag{4}$$

$$\frac{B}{C} = 3h - s \tag{5}$$

As detailed in the Part 2 to Part 4 of ESI and supported by the extensive experimental data (Figs. S2–S6, S9–S11 and Table S2 in ESI), the optimized experimental parameters and the subsequent validation of quantitative accuracy ensure that the systematic error remains within a reasonable and acceptable threshold (less than 5%), thereby demonstrating the high reliability and robustness of this methodology. Following the integration of the corresponding resonances in the ^{1}H- and ^{29}Si-NMR spectra for samples P-1 to P-5 (Figs. 9A and 9B), the h and s values were determined. By substituting these experimental values into Eqs. (4) and (5), the precise molar ratios of the Si-centered structural units were calculated for all the five PHPS samples, as summarized in Table 1.

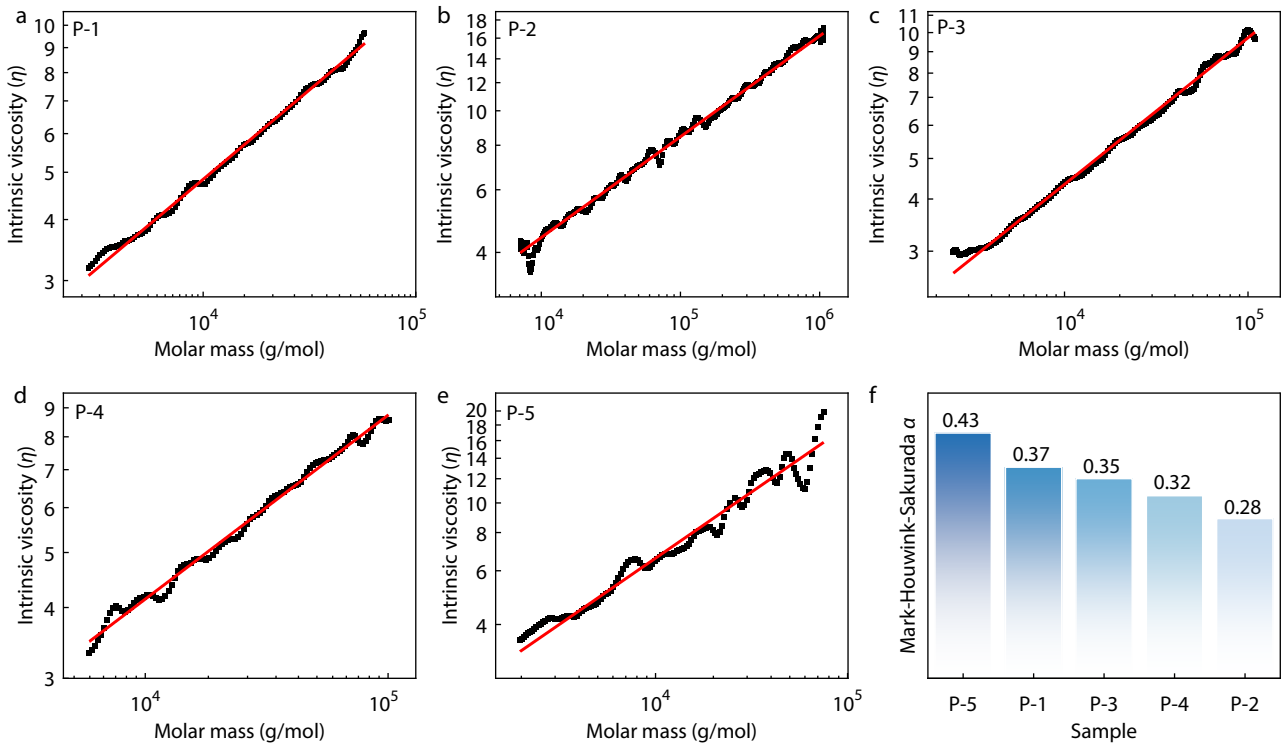

Fig. 8 (a–e) Mark-Houwink plots of samples P-1 to P-5; (f) Comparison of α values among P-1 to P-5.

https://doi.org/10.1007/s10118-026-3804-5

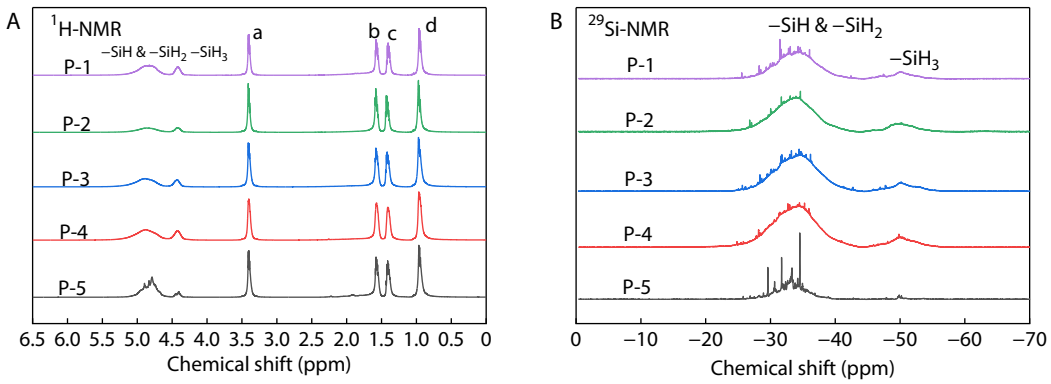

Fig. 9 Dual-nuclear quantitative NMR characterization of samples P-1 to P-5: (A) quantitative ^{1}H-NMR; (B) quantitative ^{29}Si-NMR.

Table 1 Calculated relative molar fractions of five chain units in samples P-1 to P-5.

	h	*s*	*A*	*B*	*C*	*D*	*E*
P-1	3.89	7.75	3.83	3.92	1.00	1.12	6.03
P-2	2.89	6.86	5.05	1.81	1.00	0.85	6.02
P-3	3.79	7.71	4.05	3.66	1.00	0.71	6.35
P-4	3.21	7.25	4.87	2.38	1.00	0.73	6.30
P-5	9.43	16.00	3.71	12.29	1.00	1.96	10.93

Building on the quantitative resolution of the Si-centered units, the molar ratios of the N-centered structural units (specifically —NH and —N) were further investigated. In practical applications, PHPS is typically utilized in dibutyl ether (DBE) solutions for film deposition and subsequent silica conversion. Given its pronounced thermal sensitivity, the molecular structure of PHPS may undergo undesirable changes during the physical solvent exchange processes. Therefore, despite the resonance overlap between the —NH signal of PHPS and the b, c, and d proton signals of the DBE solvent in the ^{1}H-NMR spectrum (Fig. 10), the original DBE solvent system was retained to ensure that the characterization results accurately reflect the molecular structure of the PHPS precursor under real-world application conditions.

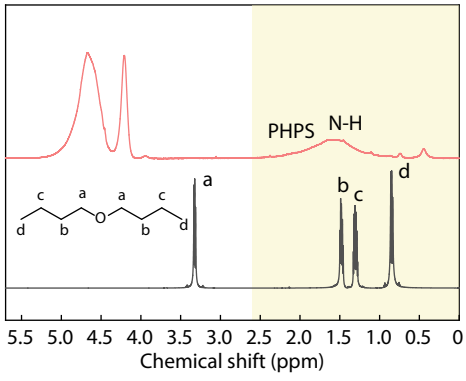

Fig. 10 Feasibility schematic of the "solvent-signal subtraction" approach used in dual-nuclear integration.

To address the challenge of spectral congestion, a solvent signal subtraction strategy was implemented for the integration of the —NH area. Since the "a" peak of DBE is distinct, it serves as a reliable internal reference to account for the solvent contribution within the overlapped region. Let "*m*" represent the integral ratio of the DBE "a" peak to the PHPS —SiH_3 peak, and "*n*" represent the ratio of the total area of the overlapped region (comprising DBE b, c, d peaks and the PHPS —NH peak) to the —SiH_3 peak area. By subtracting the calibrated solvent contribution, the relative molar ratio of —NH to —SiH_3 can be accurately obtained (Eq. 6).

$$\frac{D}{C} = n - 3.5 \times m \tag{6}$$

Following the determination of the —NH/—SiH_3 ratio and the proportions of the three Si-centered units, the relative content of the —N units was determined through the principle of Si—N bond conservation. Because the backbone of PHPS consists entirely of Si—N bonds, the total number of Si—N bonds provided by the three Si-centered moieties must balance those associated with the two N-centered units (—N and —NH). Based on this chemical bond conservation principle, the relative —N/—SiH_3 ratios for the five PHPS samples were calculated using known proportions of the other four structural units (Eq. 7), with the results summarized in Table 1. Consequently, comprehensive quantitative characterization of all potential structural units in PHPS (—SiH, —SiH_2, —SiH_3, —NH, and —N) was successfully achieved, marking the establishment of a robust and refined quantitative strategy for analyzing the fine structure of PHPS.

$$\frac{E}{C} = \left(\frac{A}{C} \times 3 + \frac{B}{C} \times 2 + 1 - \frac{D}{C} \times 2\right)/3 \tag{7}$$

As summarized in Table 2, the quantitative results for the

Table 2 Summary of quantitative fine-structure characterization results for samples P-1 to P-5.

	A	*B*	*C*	*D*	*E*	N_c	D_b
P-1	23%	26%	6%	7%	38%	280	0.6201
P-2	37%	9%	6%	6%	41%	343	0.7513
P-3	25%	24%	6%	4%	40%	299	0.6595
P-4	33%	14%	6%	4%	42%	334	0.7311
P-5	11%	43%	3%	6%	36%	229	0.4896

https://doi.org/10.1007/s10118-026-3804-5

five structural units were normalized to facilitate a more direct comparison across the samples. Specifically, the molar fraction of each individual structural unit was derived by dividing its respective molar quantity by the total molar sum of all five units within each sample.

The molar ratios of the five structural units were further normalized to enhance the comparability of the structural data (Table 2). Specifically, molar fractions were calculated by dividing the molar amount of each unit by the total molar quantity of all five units. However, these individual fractions alone do not yield a comprehensive metric that reflects the overall structural characteristics of the samples. To address this problem, two key structural parameters—number of cyclization (N_c) and degree of branching (D_b)—were derived based on the relative molar ratios to —SiH_3, providing an intuitive and quantitative representation of the PHPS molecular architecture.

The parameter N_c is adapted from the organic chemistry concept of the "degree of unsaturation"[57,58] to quantify the unsaturation levels of PHPS molecules. Based on this theoretical framework, once the chemical composition and atomic molar ratios are established, the theoretical degree of unsaturation can be determined for all corresponding structural isomers. The relative molar ratios of the five fundamental structural units have been precisely determined. However, as PHPS is a polymer characterized by significant molecular weight polydispersity ($Si_nH_nN_n$), the absolute atomic stoichiometry of the system remains indefinite. Consequently, unlike well-defined small-molecule compounds, PHPS does not possess a single, discrete degree of unsaturation.

To establish a quantitative metric suitable for cross-sample comparison, a baseline of 1000 structural units was used to statistically evaluate the atomic stoichiometry of the various PHPS samples. Under this unified baseline, the relative quantities of silicon (*a*), nitrogen (*b*), and hydrogen (*c*) atoms can be uniquely determined based on the previously resolved molar ratios of the five structural units. Given that the chemical characteristics of PHPS preclude the existence of double or triple bonds, the degree of unsaturation is entirely attributed to the formation of cyclic structures. Therefore, by substituting the aforementioned atomic ratios into the unsaturation formula (Eq. 8), a unique "ring count" can be calculated for each PHPS sample. In summary, this "ring count" is defined as the average number of rings formed per 1000 randomly selected structural units, serving to quantitatively characterize the density of cyclic structures within the molecular network (Eq. 9).

$$U = N_c = [(2 \times A + B - C) + 2]/2 \tag{8}$$

$$N_c = 1000 \times \frac{(A + B + C) \times 2 + (D + E) - (A + B \times 2 + C \times 3 + D) + 2}{2 \times (A + B + C + D + E)} \tag{9}$$

The degree of branching (D_b) is defined as the fraction of the two types of branching nodes (—SiH and —N) relative to the total number of structural units, quantitatively reflecting the extent of three-dimensional networking (Eq. 10). The structural parameters of the five PHPS samples are presented in Table 2. As indicated, sample P-2 exhibits the highest b and U values among the five samples, signifying the most extensive 3D networking and the densest cyclic architecture. In contrast, sample P-5 shows the lowest values for both parameters, with the other samples falling between these two extremes. Notably, the branching degree and number of cyclization of P-2 are approximately 53% and 49% higher than those of P-5, respectively. Through this refined quantitative characterization and parameterization, the previously qualitative descriptions of the PHPS have been transformed into comparable quantitative indicators. This advancement not only completes the comprehensive characterization strategy for PHPS but also provides a robust parameter-based foundation for future investigations into structure-property relationships.

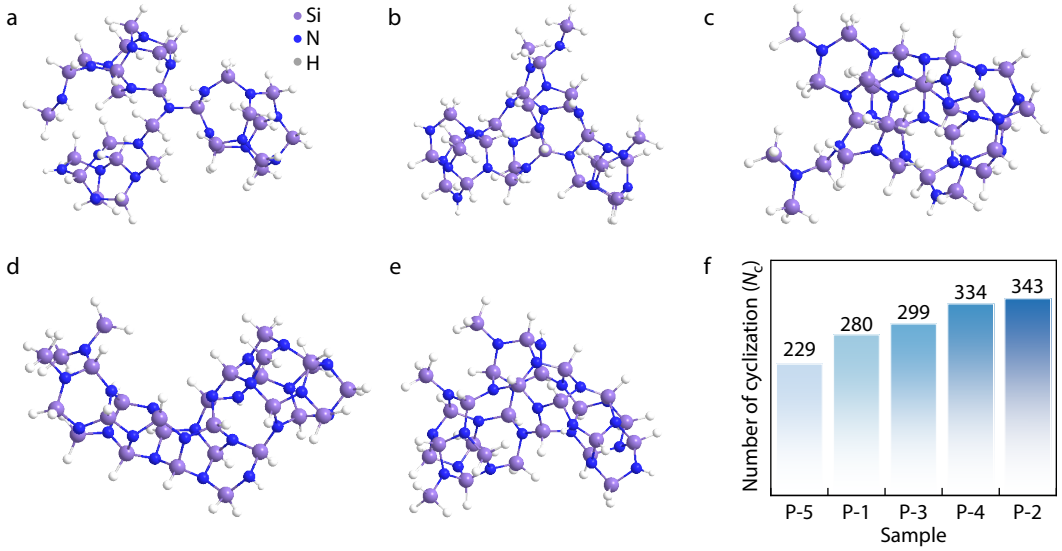

Fig. 11 (a–e) Representative three-dimensional molecular conformations of samples P-5, P-1, P-3, P-4, P-2; (f) Comparison of the number of cyclization (N_c) among samples P-1 to P-5.

$$D_b = \frac{A + E}{A + B + C + D + E} \quad (10)$$

3D Molecular Structure Simulation of PHPS

Finally, representative molecular models were constructed for various PHPS samples to provide a visual representation of the quantitative structural parameters. Three-dimensional (3D) conformations were optimized *via* DFT simulations to elucidate architectural differences and conformational transitions at the molecular scale.

As illustrated by the simulation results (Figs. 11a–11f), the molecular configurations and topological networks exhibit significant variations that are highly consistent with the established fine-structural parameters. Specifically, the model for sample P-5 displays a predominantly extended conformation with sparse interconnecting nodes and low spatial connectivity, manifesting a distinct linear-ring structural character. In contrast, the model for sample P-2 shows a markedly increased proportion of cyclic structures, with a backbone defined by multi-point linkages and multi-ring coupling, resulting in a highly networked cage-like architecture. This compact spatial packing likely exposes a higher density of potential reactive sites, such as terminal groups or active Si—H moieties, on the molecular surface, potentially leading to enhanced structural reactivity. The remaining samples (P-1, P-3, and P-4) exhibit transitional features, with intermediate levels of localized cyclization and networking.

From the perspective of topological evolution, systems with lower number of cyclization are primarily composed of linear-ring structures. As the number of cyclization increases, the probability of cyclization and multi-point branching rises significantly, driving the molecular architecture toward a cage-like network characterized by higher connectivity and intensified spatial constraints. This molecular-level structural evolution provides a direct theoretical basis for interpreting the macroscopic performance variations observed across the different PHPS samples.

CONCLUSIONS

In summary, by addressing the challenges of high structural polydispersity and the difficulty in quantifying the fine structure of PHPS, this work establishes a comprehensive framework for the fine structural elucidation of PHPS. To overcome the limitations of conventional idealized descriptions, we propose a methodology centered on "characteristic atom-centered structural units." By integrating multidimensional NMR (HSQC and HMBC), multi-angle DEPT techniques, and GPC-MALS-Vis, the unambiguous identification of three Si-centered units (—SiH, —SiH_2, and —SiH_3) and two N-centered units (—N and —NH) was achieved, along with the establishment of a robust strategy for evaluating the branching architecture of PHPS. Furthermore, a quantitative resolution strategy was developed by simultaneously solving quantitative ^{1}H- and ^{29}Si-NMR data coupled with chemical bond conservation principles, enabling precise molar quantification of all five fundamental structural units. On this basis, two novel structural parameters—number of cyclization (N_c) and branching degree (D_b)—were introduced, and DFT-based 3D molecular modeling was utilized to demonstrate the complex conformations of the PHPS framework. Overall, the systematic characterization strategy developed in this study provides a solid theoretical and experimental foundation for the rational design and future exploration of structure-property relationships in PHPS-based materials.

BIOGRAPHY

2026 Rising Scholar: Zong-Bo Zhang is a Professor and PhD supervisor at the Institute of Chemistry, Chinese Academy of Sciences, where he currently serves as a Principal Investigator in the Laboratory of Polymer Materials for Extreme Environments. His research interests focus on synthesis and application of polymer-derived ceramic precursors. Prof. Zhang has made significant breakthroughs in the synthesis of silicon-containing polymeric precursors and promoting theirs large-scale application as matrix for ceramic composites, high-temperature resistant adhesives and functional coatings . He has published over 50 papers and filed more than 30 patents.

Conflict of Interests

The authors declare no interest conflict.

Electronic Supplementary Information

Electronic supplementary information (ESI) is available free of charge in the online version of this article at http://doi.org/10.1007/s10118-026-3804-5.

Data Availability Statement

The data supporting the findings of this study are available from the corresponding author upon reasonable request.

ACKNOWLEDGMENTS

A portion of this work was based on data obtained from the Nuclear Magnetic Resonance Technology Group of the Institute of Chemistry, Chinese Academy of Sciences. The authors gratefully acknowledge the cooperation of the NMR scientists at the Nuclear Magnetic Resonance Technology Group. This study was financially supported by the National Natural Science Foundation of China (No. 52402368).

REFERENCES

1 Fu, S.; Zhu, M.; Zhu, Y. Organosilicon polymer-derived ceramics: An overview. *J. Adv. Ceram.* **2019**, *8*, 457–478.
2 Vakifahmetoglu, C.; Menapace, I.; Hirsch, A.; Biasetto, L.; Hauser, R.; Riedel, R.; Colombo, P. Highly porous macro-and microcellular ceramics from a polysilazane precursor. *Ceram. Int.* **2009**, *35*, 3281–3290.
3 Stock, A.; Somieski, K. Siliconhydrides X. Nitrogen-containing Compounds. *Chem. Ber* **1921**, *54*, 740–758.
4 Seyferth, D.; Wiseman, G. H.; Prud'homme, C. A liquid silazane precursor to silicon nitride. *J. Am. Ceram. Soc.* **1983,** *66*, C–13–C–14.
5 Okamura, T.; Kanda, T.; Sakurai, I.; Barnickel, B. B.; Aoki, H., Perhydropolysilazane, composition containing same, and

Graphical Abstract

A Multidimensional and Multinuclear Nuclear Magnetic Resonance Spectroscopy Strategy for Fine Structural Elucidation of Perhydropolysilazane

Li-Fei Yuan, Qian Li, Hui-Yuan Yang, Ji-Lei Chen, Ding-Yu Hou, Peng-Fei Li, Cai-Hong Xu, and Zong-Bo Zhang

Institute of Chemistry, Chinese Academy of Sciences; University of Chinese Academy of Sciences

A systematic strategy for the fine-structure characterization of perhydropolysilazane (PHPS) is established. By introducing structural parameters—degree of branching and number of cyclization—the complex molecular structure of PHPS is quantitatively resolved, providing a robust framework for its detailed structural elucidation.

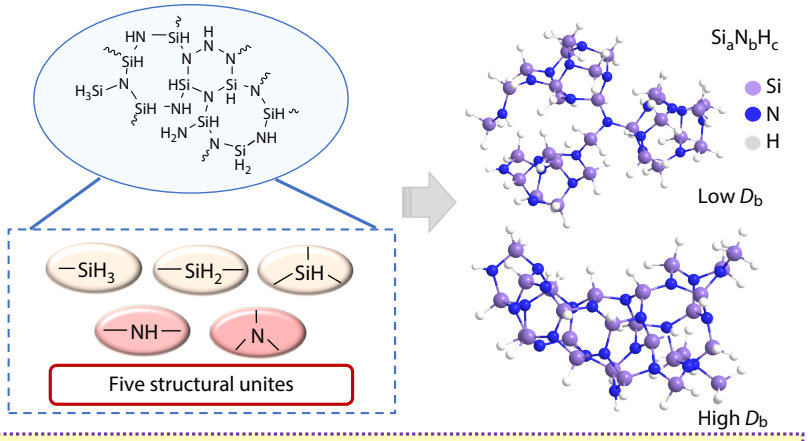

Structural parameters: Degree of branching (D_b)$=\frac{A+B}{A+B+C+D+E}$

Number of cyclization (N_c)$=1000\times\frac{(A+B+C)\times2+(D+E)-(A+B\times2+C\times3+D)+2}{2\times(A+B+C+D+E)}$

PS: Consider a PHPS sample containing *A*, *B*, *C*, *D* and *E* moles of —SiH, —SiH_2, —SiH_3, —NH and —N, respectively.

Chinese J. Polym. Sci. 2026 *https://doi.org/0.1007/s10118-026-3804-5*

method for forming silica film using same. **2017**, United States, US9793109B2.

6 Yokoyama, Y.; Nanba, T.; Yasui, I.; Kaya, H.; Maeshima, T.; Isoda, T. X-ray diffraction study of the structure of silicon nitride fiber made from perhydropolysilazane. *J. Am. Ceram. Soc.* **1991**, *74*, 654–657.

7 Funayama, O.; Tashiro, Y.; Kamo, A.; Okumura, M.; Isoda, T. Conversion mechanism of perhydropolysilazane into silicon nitride-based ceramics. *J. Mater. Sci.* **1994**, *29*, 4883–4888.

8 Sato, K.; Kaya, H.; Funayama, O.; Isoda, T. Evaluation of polysilazanes-perhydropolysilazane, polyborosilazane and methylhydropolysilazane-as matrix precursors of ceramic-matrix composites. *J. Ceram. Soc. Jpn.* **2001**, *109*, 440–446.

9 Wang, W. Y.; Zhang, Y. L.; Guo, X.; Wang, L. M.; Zhang, J. R.; Yang, H.; Dong, G. J.; Zhang, Z. B.; Xu, C. H. Rapid conversion of perhydropolysilazane into thin silica coating at low temperature. *Chinese J. Polym. Sci.* **2023**, *41*, 1198–1205.

10 Yue, S.; Wang, S.; Han, D.; Huang, S.; Xiao, M.; Meng, Y. Perhydropolysilazane-derived-SiO_x coated cellulose: a transparent biodegradable material with high gas barrier property. *Cellulose* **2022**, *29*, 8293–8303.

11 Chen, Q.; Zhang, X.; Wang, F. Experimental study of thermal diffusion enhanced vapor transfer performance with perhydropolysilazane-derived silica (PDS) coating membranes in air dehumidification process. *Int. J. Refrig.* **2021**, *122*, 21–32.

12 Song, L.; Sun, H.; Suzuri, Y. Polysilazane-coated films achieving record-high moisture barrier performance with sub-10 seconds densification using high-power VUV irradiation. *Adv. Sci.* **2025**, *12*, 2415721.

13 Günthner, M.; Kraus, T.; Dierdorf, A.; Decker, D.; Krenkel, W.; Motz, G. Advanced coatings on the basis of Si (C) N precursors for protection of steel against oxidation. *J. Eur. Ceram. Soc.* **2009**, *29*, 2061–2068.

14 Zhang, Y.; Wang, W.; Li, P.; Wang, L.-M.; Zhang, J.; Li, X.; Zhang, Z.; Xu, C. Thermal conversion process of tetraethyl orthosilicate-based silica sol and perhydropolysilazane into inorganic silica films. *Cryst. Growth Des.* **2023**, *23*, 5965–5974.

15 Sønderbæk-Jørgensen, R. Polysilazanes for coating applications. Thesis, Technical University of Denmark, **2022**.

16 Naganuma, Y.; Kato, C.; Watanabe, T.; Kaneko, S.; Tanaka, S. Physicochemical and structural properties of silica films prepared from perhydropolysilazane using vacuum ultraviolet irradiation.

Thin Solid Films **2024**, *802*, 140453.
17 Zhang, T.T.; Zhou, M. X.; Guo, Z. Y.; Zhao, Y. B.; Han, D.; Xiu, H.; Bai, H. W.; Zhang, Q.; Fu, Q. Improving impact toughness of polylactide/ethylene-co-vinyl-acetate blends *via* adding fumed silica nanoparticles: effects of specific surface area-dependent interfacial selective distribution of silica. *Chinese J. Polym. Sci.* **2021**, *39*, 1040–1049.
18 Fan, L. L.; Quan, J. Y.; Zhang, H.; Yu, J. R.; Hu, Z. M.; Wang, Y. Preparation of hydrophilic UHMWPE hollow fiber membranes by chemically bounding silica nanoparticles. *Chinese J. Polym. Sci.* **2021**, *39*, 189–200.
19 Takeuchi, K.; Nemoto, D.; Suga, T.; Higurashi, E. in *Formation of SiO_2 bonding interface using perhydropolysilazane at room temperature*, 2024 ICEP, IEEE, **2024**, pp. 113–114.
20 Nemoto, D.; Takeuchi, K.; Higurashi, E. In *Investigation of plasma gases for polysilazane conversion into SiO_2 for wafer bonding*, 2024 ICEP, IEEE, **2024**, pp. 289–290.
21 Takeuchi, K.; Suga, T.; Higurashi, E. Room temperature wafer bonding through conversion of polysilazane into SiO_2. *Sci. Rep.* **2024**, *14*, 1267.
22 Wang, W.; Tamakloe, S.; Deng, Z.; Li, L.; Cai, W.; Lu, K. Effects of processing temperature on the corrosion and tribocorrosion resistance of perhydropolysilazane-derived coatings on AISI 304 steel. *Surf. Coat. Technol.* **2022**, *439*, 128463.
23 Li, P.; Wang, D.; Zhang, Z.; Guo, Y.; Jiang, L.; Xu, C. Room-temperature, solution-processed SiO_x *via* photochemistry approach for highly flexible resistive switching memory. *ACS Appl. Mater. Interfaces* **2020**, *12*, 56186–56194.
24 Li, P.; Zhang, Y.; Guo, Y.; Jiang, L.; Zhang, Z.; Xu, C. Resistance switching behavior of a perhydropolysilazane-derived SiO_x-based memristor. *J. Phys. Chem. Lett.* **2021**, *12*, 10728–10734.
25 Riffard, F.; Joannet, E.; Buscail, H.; Rolland, R.; Perrier, S. Beneficial effect of a pre-ceramic polymer coating on the protection at 900 C of a commercial AISI 304 stainless steel. *Oxid. Met.* **2017**, *88*, 211–220.
26 Bawane, K.; Lu, K.; Li, Q.; Bordia, R. High temperature oxidation behaviors of SiON coated AISI 441 in $Ar+O_2$, $Ar+H_2O$, and $Ar+CO_2$ atmospheres. *Corros. Sci.* **2020**, *166*, 108429.
27 Baek, J. J.; Park, S. M.; Kim, Y. R.; Chang, K. C.; Heo, Y.-J.; Bae, G. Y.; Choi, K. H.; Shin, G. Intense pulsed UV light treatment to design functional optical films from perhydropolysilazane: an alternative to conventional heat treatment processes. *J. Mater. Sci.* **2022**, *57*, 254–273.
28 Zhang, Z.; Shao, Z.; Luo, Y.; An, P.; Zhang, M.; Xu, C. Hydrophobic, transparent and hard silicon oxynitride coating from perhydropolysilazane. *Polym. Int* **2015**, *64*, 971–978.
29 Kobayashi, Y.; Yokota, H.; Fuchita, Y.; Takahashi, A.; Sugahara, Y. Characterization of gas barrier silica coatings prepared from perhydropolysilazane films by vacuum ultraviolet irradiation. *J. Ceram. Soc. Jpn.* **2013**, *121*, 215–218.
30 Channa, I. A.; Shah, A. A.; Rizwan, M.; Makhdoom, M. A.; Chandio, A. D.; Shar, M. A.; Mahmood, A. Process parameter optimization of a polymer derived ceramic coatings for producing ultra-high gas barrier. *Materials* **2021**, *14*, 7000.
31 Ackley, B. J.; Martin, K. L.; Key, T. S.; Clarkson, C. M.; Bowen, J. J.; Posey, N. D.; Ponder Jr, J. F.; Apostolov, Z. D.; Cinibulk, M. K.; Pruyn, T. L. Advances in the synthesis of preceramic polymers for the formation of silicon-based and ultrahigh-temperature non-oxide ceramics. *Chem. Rev.* **2023**, *123*, 4188–4236.
32 Bender; Chin, W.; Banaszak Holl, M. M. Synthesis and Characterization of a Soluble, Highly Branched Organo-Silicon–Nitride Polymer. *Chem. Mater.* **1999**, *11*, 154–157.
33 Chen, J.; Li, H.; Kao, K.; Lin, W.; Xiong, Y.; Huang, Z. Facile synthesis of a novel transparent melt-spinnable polysilazane. *Nano Sel.* **2022**, *3*, 834–840.
34 Barysheva, A.; Mochalov, G.; Suvorov, S. Synthesis of polysilazane by ammonolysis of dichlorosilane in a nucleophilic solvent. *Russ. J. Appl. Chem.* **2021**, *94*, 1226–1231.
35 Isoda, T.; Kaya, H.; Nishii, H.; Funayama, O.; Suzuki, T.; Tashiro, Y. Perhydropolysilazane precursors to silicon nitride ceramics. *J. Inorg. Organomet. Polym.* **1992**, *2*, 151–160.
36 Rappé, A. K.; Casewit, C. J.; Colwell, K. S.; Goddard III, W. A.; Skiff, W. M. UFF, a full periodic table force field for molecular mechanics and molecular dynamics simulations. *J. Am. Chem. Soc.* **1992**, *114*, 10024–10035.
37 M.J. Frisch, G. W. T., H.B. Schlegel, G.E. Scuseria, M.A. Robb, J.R. Cheeseman, G. Scalmani, V. Barone, G.A. Petersson, H. Nakatsuji, X. Li, M. Caricato, A.V. Marenich, J. Bloino, B.G. Janesko, R. Gomperts, B. Mennucci, H.P. Hratchian, J.V. Ortiz, A.F. Izmaylov, J.L. Sonnenberg, D. Williams-Young, F. Ding, F. Lipparini, F. Egidi, J. Goings, B. Peng, A. Petrone, T. Henderson, D. Ranasinghe, V.G. Zakrzewski, J. Gao, N. Rega, G. Zheng, W. Liang, M. Hada, M. Ehara, K. Toyota, R. Fukuda, J. Hasegawa, M. Ishida, T. Nakajima, Y. Honda, O. Kitao, H. Nakai, T. Vreven, K. Throssell, J.A. Montgomery, J.E. Peralta, F. Ogliaro, M.J. Bearpark, J.J. Heyd, E.N. Brothers, K.N. Kudin, V.N. Staroverov, T.A. Keith, R. Kobayashi, J. Normand, K. Raghavachari, A.P. Rendell, J.C. Burant, S.S. Iyengar, J. Tomasi, M. Cossi, J.M. Millam, M. Klene, C. Adamo, R. Cammi, J.W. Ochterski, R.L. Martin, K. Morokuma, O. Farkas, J.B. Foresman, D.J. Fox *Gaussian~16 Revision B.01*, Gaussian, Inc.: Wallingford CT, **2016**.
38 Stewart, J. J. Optimization of parameters for semiempirical methods V: Modification of NDDO approximations and application to 70 elements. *J. Mol. Model.* **2007**, *13*, 1173–1213.
39 Seyferth, D.; Wiseman, G. H.; Prud'homme, C., Silicon-nitrogen polymers and ceramics derived from reactions of dichlorosilane, H_2SiCl_2. In *Emergent process methods for high-technology ceramics*, Springer, **1984**, pp. 263–269.
40 Funayama, O.; Aoki, T.; Kato, T.; Okoda, M.; Isoda, T. Synthesis of thermosetting copolymer of polycarbosilane and perhydropolysilazane. *J. Mater. Sci.* **1996**, *31*, 6369–6375.
41 Rochow, E. G. The chemistry of silicones. *Scientific American* **1948**, *179*, 50–53.
42 Brook, A. G. in *Silicon in organic, organometallic, and polymer chemistry*. John Wiley & Sons, New York, **2000**.
43 Birot, M.; Pillot, J. P.; Dunogues, J. Comprehensive chemistry of polycarbosilanes, polysilazanes, and polycarbosilazanes as precursors of ceramics. *Chem. Rev.* **1995**, *95*, 1443–1477.
44 Brunet, F.; Bertani, P.; Charpentier, T.; Nonat, A.; Virlet, J. Application of ^{29}Si homonuclear and $^{1}H-^{29}Si$ heteronuclear NMR correlation to structural studies of calcium silicate hydrates. *J. Phys. Chem.* **2004**, *108*, 15494–15502.
45 Takeuchi, Y.; Takayama, T. ^{29}Si-NMR spectroscopy of organosilicon compounds. *Chem. Org. Silicon Compd.* **1998,** *2*, 267–354.
46 Smith, K. A.; Kirkpatrick, R. J.; Oldfield, E.; Henderson, D. M. High-resolution silicon-29 nuclear magnetic resonance spectroscopic study of rock-forming silicates. *Am. Mineral.* **1983**, *68*, 1206–1215.
47 Scholl, R. L.; Maciel, G. E.; Musker, W. K. Silicon-29 chemical shifts of organosilicon compounds. *J. Am. Chem. Soc.* **1972**, *94*, 6376–6385.
48 Brunet, F. Polymerization reactions in methyltriethoxysilane studied through ^{29}Si-NMR with polarization transfer. *J. Non-Cryst. Solids* **1998**, *231*, 58–77.
49 McDonnell, P. A.; Gauthier, A. D.; Ferro, M. P. Differentiation of regioisomers at ^{15}N natural abundance using gradient-enhanced $^{1}H/^{15}N$ HMBC NMR spectroscopy. *Magn. Reson. Chem.* **1998**, *36*, 35–38.
50 Gill, B.; Manley-Harris, M.; Thomson, R. Use of natural abundance ^{15}N DEPT NMR to investigate curing of urea–formaldehyde resin

in the presence of wood fibers. *Magn. Reson. Chem.* **2003**, *41*, 622–625.
51 Martin, G. J.; Martin, M. L.; Gouesnard, J. P. in *^{15}N-NMR spectroscopy*. Springer Science & Business Media, **2012**.
52 Marek, R.; Lycka, A. ^{15}N NMR spectroscopy in structural analysis. *Curr. Org. Chem*. **2002,** *6*, 35–66.
53 Blinka, T. A.; Helmer, B. J.; West, R., Polarization transfer NMR spectroscopy for silicon-29: the INEPT and DEPT techniques. In *Adv. Organomet. Chem*., Elsevier, **1984**, Vol. 23, pp. 193–218.
54 Zimm, B. H.; Stockmayer, W. H. The dimensions of chain molecules containing branches and rings. *J. Phys. Chem.* **1949**, *17*, 1301–1314.
55 Stockmayer, W. H.; Fixman, M. Dilute solutions of branched polymers. *Ann. N. Y. Acad. Sci.* **1953**, *57*, 334–352.
56 Wyatt, P. J. Light scattering and the absolute characterization of macromolecules. *Anal. Chim. Acta* **1993**, *272*, 1–40.
57 Crews, P.; Rodriquez, J.; Jaspars, M.; Crews, R. J. in *Organic structure analysis*. Oxford University Press, New York, **2010**.
58 Badertscher, M.; Bischofberger, K.; Munk, M. E.; Pretsch, E. A novel formalism to characterize the degree of unsaturation of organic molecules. *J. Chem. Inf. Comput. Sci.* **2001**, *41*, 889–893.

https://doi.org/10.1007/s10118-026-3804-5